Manuscript:

In Vitro Degradation and Mechanical Properties of PLA-PCL Copolymer Unit Cell Scaffolds Generated by Two-Photon Polymerization

R. M. Felfel[1,4], Leander Poocza[2], Miquel Gimeno-Fabra[1,] Tobias Milde[2], Gerhard Hildebrand[2], Ifty Ahmed[1], Colin Scotchford[1], Virginie Sottile[3], David Grant[1,**], Klaus Liefeith[2,*]

[1]Division of Materials Mechanics and Structures, Faculty of Engineering, University of Nottingham, UK
[2]Institute for Bioprocessing and Analytical Measurement Techniques e.V., 37083 HeilbadHeiligenstadt, Germany
[3]Wolfson STEM Centre, School of Medicine, University of Nottingham, UK
[4]Physics Department, Faculty of Science, Mansoura University, 35516, Egypt

Abstract:

The manufacture of 3D scaffolds with specific controlled porous architecture, defined microstructure and an adjustable degradation profile was achieved using two-photon polymerization (2PP) with a maximal size of 2x4x2 mm³. Scaffolds made from poly(D,L-lactide-co-ε-caprolactone) copolymer with varying lactic acid (LA) and ε -caprolactone (CL) ratios (16:4, 18:2 and 9:1) were generated via ring-opening-polymerization and photoactivation and coded LC16:4, 18:2 and 9:1. The reactivity was quantified using photo-DSC, yielding a double bond conversion ranging from 70% to 90%. All materials were suitable for defined microstructuring of reproducible porous scaffolds. The pore sizes for all LC scaffolds were *ca.* 300 µm and throat sizes varied from 152 to 177 µm. *In vitro* degradation was conducted at body and elevated temperatures; 37, 50 and 65ºC and activation energies for the scaffold materials were determined using an Arrhenius equation. Change in compressive properties immersed at 37ºC over time was also measured. Variations in thermal, degradation and mechanical properties of the LC scaffolds were related to the LA/CL ratio. Scaffold LC 16:4 showed significantly lower glass transition temperature (T_g) (4.8ºC) in comparison with the LC 18:2 and 9:1 (ca. 32ºC). Rates of mass loss for the LC16:4 scaffolds at all temperatures were significantly lower than that for LC18:2 and 9:1. The degradation activation energies ranged from 82.7 to 94.9 kJ mol^{-1}. A prediction for degradation time was applied through a correlation between long-term degradation studies at 37ºC and short-term studies at elevated temperatures (50 and 65ºC) using the half-life of mass loss (Time ($M_{1/2}$)) parameter. However, the initial compressive moduli for LC18:2 and 9:1 scaffolds were 7 to 14 times higher than LC16:4 (ca. 0.27) which was suggested to be due to

its higher CL content (20%). All scaffolds showed a gradual loss in their compressive strength and modulus over time as a result of increasing mass loss over time. The manufacturing process utilized and the scaffolds produced have vast potential for use in tissue engineering and regenerative medicine applications.

Keywords: Scaffolds, Stereo-lithography, Photopolymerization, Conversion, Degradation, Activation Energy, Compressive properties.

Corresponding Authors:
* Prof. Dr. Klaus Liefeith
klaus.liefeith@iba-heiligenstadt.de

** Prof. David Grant
david.grant@nottingham.ac.uk

Introduction:

Biocompatible and biodegradable polymers have become commonplace for several biomedical applications such as tissue engineering scaffolds for regenerative medicine [1, 2], particulate carriers for drug delivery and targeted therapeutics as well as for bioactive coatings [2-4]. Traditional scaffold fabrication techniques have included the production of porous polymer constructs by freeze-extraction and –gelation [5], electrospinning [6], melt electrospinning [7, 8] or with hydrogels [9-12] as substrates for cell attachment. However, complex architectures with specifically controlled micro- and macro-scale features have been difficult to achieve. Recent trends have focused on preparing multifunctional monomers which contain reactive groups (acrylates) to form cross-linked scaffolds of predefined microstructures using CAD-based manufacturing technologies [11]. Fabrication of hierarchical 3D scaffold constructs for tissue engineering, have been manufactured via 3D-printing [13], 3D-plotting [14] and stereo-lithography [15]. Resolutions of up to 50 µm have been achieved using photo-polymerization techniques for the spatial patterning of materials in a layer-by-layer approach by stereo-lithography [16]. Generation of complex structures with high resolution and without the necessity of photomasks are the major advantages of direct laser writing techniques compared to traditional lithography methods. However, higher resolutions can be obtained by making use of two-photon absorption (TPA), an effect which was described theoretically in 1931 by Göppert-Mayer [17],

but has only been translated into an application in the last decade. For TPA, excitation wavelengths in the near-infrared (NIR) were used. This low energy of photons makes a simultaneous TPA necessary for excitation of the photoinitiator (see Figure 1A). For sufficient photon density, femtosecond laser pulses are used. The long wavelength of the NIR allows for deeper penetration into the material and thus structuring in millimeter dimensions and a submicron resolution (Figure 1B) [18-22]. The approach described here generated a scaffold for bone tissue engineering aiming to address critical size defects, offering a slow degradation rate, appropriate for bone regeneration, and provide features enabling angiogenesis and stress distribution accompanied with high loads present in bone.

The degradation rate of degradable polymers is controlled by numerous factors such as degree of crystallinity, chemical structure, molecular weight, porosity, surface/volume ratio, manufacturing methods, implantation site, applied load, degradation temperature and pH of the degradation medium [23-26]. Degradation temperature has a significant influence on the degradation of biodegradable polymers. The rate of hydrolysis is known to increase with degradation temperature which would potentially make the correlation between short-term effects at high temperature and long-term effects at physiological temperature achievable. Moreover, body temperature varies significantly between human and certain animals such as pigs and rabbits (approximately 1-3^{o}C higher than human temperature) which are commonly used as *in vivo* models [23].

The main purpose of accelerated degradation studies is to attain degradation profiles within a shorter period of time and descriptive to that obtained at standard degradation conditions [24]. Depending on the polymer and geometry, degradable devices can take up to several years for complete degradation at physiological temperature (37^{o}C). Therefore, validated accelerated degradation studies are an attractive research tool [27] to explore the influence of the physico-chemical factors as well as other influences such as initiators and polymer blends.

For example a comparison of flexural strength of PLA pins degraded at 37^{o}C and 70^{o}C in saline solution (NaCl) was performed by Claes *et al*. [28]. They found that the pins completely lost their flexural strength after 18 months and 96 hours of immersion in NaCl at 37^{o}C and 70^{o}C respectively. It was concluded that accelerated degradation tests can be afforded an expectation of degradation profiles in a short period of time by correlating the results of the 70^{o}C test with

that obtained at 37ºC. Deng *et al.* [29] investigated tensile properties of poly(glycolide-co-L-lactide) (PGLA) multifilament braids over time in phosphate buffered saline (PBS) solution at different temperatures (from 27.5 to 47.5ºC with 5ºC increments). A rapid loss of tensile strength was seen for specimens degraded at higher temperatures. Tensile strength of the braids decreased by ~10% after soaking in PBS for 10 days at 47.5ºC. However, 30 days were required to reach 10% loss in the strength at 37ºC. The time required to reach a given breaking strength at different temperature followed an Arrhenius equation and the activation energies calculated were 96.12 to 102.38 kJ mol^{-1}.

In the present study, porous 3D scaffolds based on poly(D,L-lactide-co-ε-caprolactone) (PLCL) copolymer with different compositions of (LC16:4, LC18:2 and LC9:1) were manufactured via two photon polymerization technology in dimensions of 2x2x4 mm^3 (see Figure 1C). The 3D scaffold structures were based on a Schwarz Primitive (P) minimal surface derived unit cells. By combining the unit cells, a scaffold of controlled pore size, porosity and dimensions was generated. In vitro degradation was conducted for the scaffolds at varying temperatures (37, 50 and 65ºC). The retention of compressive properties of the scaffolds was also explored during immersion and at 37ºC for 83 days. Furthermore, the influence of change in the composition and chain length of the lactide-caprolactone containing precursor material on scaffold properties (stiffness, degradation rate) was also examined.

Materials and Methods:

ε-Caprolactone (CL, Sigma-Aldrich, 97%), diethylene glycol (DEG, Sigma-Aldrich, 99%), 3,6-dimethyl-1,4-dioxane-2,5-dione (D,L-lactide, Sigma-Aldrich), methacryloyl chloride (MACL, Sigma-Aldrich, 97%), H-methoxyphenol (MEHQ, Sigma-Aldrich, 99%), stannous 2-ethylhexanoat (Sigma-Aldrich, 95%), triethylamine (TEA, Merck, 99%), Irgacure369™ (Cibachemicals) and BA740 (Organic Chemistry Department, University of Jena) as photoinitiators were used as received without further purification. Solvents were of commercial reagent grade.

Precursor Synthesis

Synthesis of methacrylated random copolymers of lactic acid (LA) and ε-caprolactone (CL) was adapted from Davis *et al*. [30]. In brief, certain quantities of D,L-Lactide, ε-caprolactone and DEG (2.00 g, 18.85 mmol, 1 Äq) (see Table 1) were added to a 500 mL Schlenk round bottom

flask, stirred and heated to 130°C until all lactide melted. Stannous 2-ethylhexanoate (300 µL, 0.33 mmol) was then added and reacted overnight at 130°C under vacuum. After cooling to RT and flushing with argon, methylene chloride (100 mL) was added and the solution was cooled to 0°C. Primary TEA was added and followed by dropwise addition of 75 mL of dissolved MACL in methylene chloride over a period of 3 h. Afterwards, the flask was warmed to RT and left under continuous stirring overnight. The precipitate was then collected by filtration and the methylene chloride evaporated under reduced pressure. The resulting viscous liquid was dissolved in 50 mL of ethyl acetate, filtered again and added dropwise into 500 mL of n-hexane under stirring. The precipitate was taken up in methylene chloride and washed with aqueous hydrochloric acid (3%, 2x100 mL), saturated aqueous sodium bicarbonate solution and saturated aqueous sodium chloride solution (200 mL) and then dried over anhydrous sodium sulfate. Subsequently, 300 ppm of MEHQ (300 ppm) was added to the final product.

Methacrylation degree, molecular weight and average number of LA and CL units were quantified by ^{1}H-NMR analysis. A yield of 70-75% of a colorless liquid was obtained.^{1}H NMR (300 MHz, $CDCl_3$, d, ppm): 1.2–1.6 (m, CH_3- LA, -CH_2- CL), 1.8 (s, CH_3-C(=CH_2)), 2.3 (m, methylene protons adjacent to carbonyl carbon in CL), 3.6 (m, DEG ether protons), 4.0–4.2 (m, CH_2-O), 5.0 (m, LA backbone), 5.5 (s, CH_2=C), 6.2 (s, CH_2=C).

Photo-DSC

Photo-reactivity of LC-crosslinkers was characterised using photo-DSC (Netzsch Phoenix 204 F1, µ-sensor). In curing experiments, 2-10 mg samples containing 2% of Irgacure369™ were loaded in open aluminum crucibles and cured for 10 minutes at 30 °C, 50 °C and 70 °C using S2000 UV-lamp (Omni Cure). Samples were kept for 10 min at each temperature before application of UV.

The data of interest from photo-DSC measurements were the time of maximal heat production, t_{max}, measured in seconds, determined by the position of the peak maximum and the heat of polymerization, ΔH_P, measured in Joule per gram as a part of the reaction rate equation [31];

$$R_P = \frac{dH}{dt} \cdot \frac{1}{\Delta H_P \cdot m} \qquad (1)$$

and determined by peak integration. Measurements of the molar heat of polymerization (J/mol) were calculated on the basis of the molecular weight and degree of methacrylation determination

of NMR-analysis. The heat of the samples $\Delta H_{sample}(t)$ was calculated as follows, where 2 is the theoretical number of methacryl groups with respect to the methacrylation degree $\%_{MA}$ multiplied with the theoretical heat of a methacryl group ΔH_{MA} (55 kJ/mol) [32], divided by the molecular weight of the sample M_{sample}.

$$\Delta H_{sample}^{theo} = \frac{2 \cdot \%_{MA} \cdot \Delta H_{MA}}{M_{sample}} \qquad (2)$$

The degree of double bond conversion was then calculated with equation (3):

$$\alpha = \frac{\Delta H_{sample}^{DSC}}{\Delta H_{sample}^{theo}} \cdot 100 \qquad (3)$$

TPP structuring of LC scaffolds

For processing the precursor LCs were mixed with BA740 dissolved in acetone (0.2 mg/µL) to a final concentration of 0.2% and stirred overnight at 60°C to ensure good distribution and evaporation of excess solvent.

The TPP apparatus (M3DL, LZH Hannover, Germany) equipped with a femtosecond laser source with 800 nm wavelength, delivering trains of 140 fs pulses at 80 MHz repetition rate (VISION II, Coherent, Scotland). The beam was focused by an x63 objective lens with NA 0.75 (LD-Plan-NEOFLUAR, Zeiss, Germany) into the photoresist. Structures were produced by moving the sample with a three axis nano-positioning stage according to the computer model supported by a galvano-scanner (Aerotech, USA). The cw-Power levels of 180 mW were used for writing, measured behind the objective. The Schwarz P 520 µm unit cells were arrayed to the final dimension of 2x4x2 mm³ with an overlay of 10 µm between the cells.

Scanning electron microscopy (SEM)

Morphology of the produced scaffolds was examined using SEM (JEOL 6400) with working distance of 20 mm and an accelerating voltage of 10 kV in secondary electron imaging mode (SE). Samples were sputter-coated with platinum for 90 s at 2.2 kV. Top surfaces of the scaffolds were scanned. Size of pores and pore throats of LC scaffolds were measured using Image J 1.42 q software. Pore size was determined as average diameter of all maximal fitted spheres for each individual pore, whilst throat size represented the mean diameter of maximal spheres inscribed at the junctions between every two pores (see Figure 4). Aspect ratios of the pores, the ratio of

minor to major axes of the pore, were also determined. A total of 20 measurements were taken and results were reported by mean values ± standard deviation.

Sterilization of Scaffolds

All the manufactured LC scaffolds were kept in a well plate and packed in Tyvek® sterilization pouches (Westfield Medical Ltd, UK). The samples were irradiated according to BS EN ISO 11137-2 standard [33] with a dose of 25 ± 2.5 kGy using a ^{60}Co gamma-ray source (Systagenix/GSS, UK). Scaffolds remained in sterilisation pouches prior to use.

Differential Scanning Calorimetry (DSC)

DSC analysis was performed using a DSC Q10 (TA Instrument, USA) which was calibrated using indium. Samples (~5 mg) were placed into aluminum pans and heated over a temperature range from -20 to 450 ºC at a rate of 10 ºC min^{-1} under nitrogen gas flow (50 mL min^{-1}). The resulting thermograms were analyzed using TA universal analysis 2000 software to determine the glass transition temperature (T_g) and decomposition temperature (T_d) of the scaffold.

Degradation study

The degradation study of the scaffolds was done according to the standard BS EN ISO 10993-13:2010 [34]. Scaffolds were placed individually into glass vials containing 30 ml Phosphate buffered saline (PBS) (pH =7.4 ± 0.2) solution and maintained in an oven at 37°C. At various time points the specimens were extracted with tweezers and agitated gently to remove surplus solution before weighing. The samples were placed into empty vials and inserted within a vacuum oven (Medline Scientific, UK) at 50ºC for 60 min for drying. Afterwards, the dry weight of the scaffolds was recorded and samples were then returned to vials containing PBS.

The percentage mass change was determined using the following equation;

$$\textbf{Mass loss}\ (\%) = \left[\frac{(m - m_i)}{m_i}\right] x\ \mathbf{100} \quad (4)$$

where m is the mass of degraded sample measured at time t after drying at 50 ºC in vacuum oven for 60 min and m_i is the initial mass of the sample. At each time point every scaffold was weighed and mechanically tested allowing the degradation pathway of each individual scaffold to be followed with time.

An Arrhenius equation was utilised to extrapolate results at elevated temperatures to physiological temperature [35].

$$\boldsymbol{k = Ae^{-E_a/RT}} \qquad (5)$$

where k is reaction rate which will be represented in the current study as the rate of mass loss, A is constant, E_a is the activation energy ($JK^{-1}mol^{-1}$), R is universal gas constant ($JK^{-1}mol^{-1}$) and T is the temperature in Kelvin [36].

Mechanical testing

The compressive strength and modulus were determined using a Hounsfield testing machine and the calculations were done according to the standard ASTM 1621-10: 2010 [37] at 25±1ºC. Scaffolds were inserted vertically between two flat platens of the test machine (load was applied on the cross section). A crosshead speed of 0.5 mm/min and a 5N load cell was used. The test was carried out up to 20% strain (below the yield strain of the specimens) to obviate permanent deformation within the scaffolds. The measurements were applied on dry samples of 2x4x2 mm^3 dimensions and carried out in three successive cycles with time interval of 10 min to permit scaffold recovery. At various time points the specimens were extracted and dried in vacuum oven at 50ºC for 60 min before testing. Compressive modulus was determined as the gradient of the linear portion of stress-strain curve and strength was determined as the maximum stress at 20% strain.

Optical Microscopy

Optical images of LC16:4, 18:2 and 9:1 scaffolds were captured throughout the degradation studies at different temperatures (37, 50 and 65ºC) using a Nikon digital camera (Dxm1200F, Japan) attached to Nikon microscope (Japan). The images were processed using image analysis software (Nikon ACT-1 v. 2.62, LEAD Technologies, USA).

Results and Discussion:

Material synthesis and evaluation of the writeability

LC is a copolymer constructed from diethylene glycol and two monomers D,L lactide and ε-caprolactone. Their relative monomer contents render the polymer more hydrophilic or hydrophobic and influence the degradation rate, viscosity of the precursor and mechanical behavior of the cross-linked and solidified material and degradation behaviour. Starting from the

initial composition (LC 18:2), two content modifications were synthesized with a) higher ε-caprolactone content (LC 16:4) and b) shorter chain length (LC 9:1). Due to the high viscosity of the lactide-rich modification LC 18:2, which negatively effects the processing of the crosslinker, a lactide-rich modification with lower molecular weight (LC 9:1) was synthesized. Figure 5 shows the influence of LA/CL ratio on chain length of the LC scaffolds produced.

The material synthesis has been described by Davis *et al.* [30] for the whole range of dimethacrylated caprolactone-lactide copolymers with 20 monomer units by tin catalyzed ring-opening polymerization. For TPP, only optical transparent materials are suitable and since all materials with higher caprolactone contents have the tendency to form optical disturbing crystallites at room temperature. This opacity effect increases with increasing caprolactone concentration. Therefore, lactide-rich variations were explored in this study with a LA:CL ratio of 90% (LC 18:2) or 80% (LC 16:4). In addition, the number of total monomer units added at 90% LA content were halved from 20 units in the LC 18:2 to 10 units in LC 9:1 to reduce the chain length between the cross-linking methacrylate groups and thus the resulting mesh sizes in the final structure. The results of the synthesis are summarized in LA: D,L-lactide, CL: ε-Caprolactone, TEA: trimethylamine and MACL: methacryloyl chloride

Table **2** and showed correlation with the amounts of educts used, with a deviation of no more than one monomer unit. The lactide richer derivatives (9:1 and 18:2) tended to incorporate a lactide unit more than the target value, whereas the caprolactone richer LC 16:4 had one LA unit less. This was also well correlated with the molecular weight results obtained for the LC scaffolds, as LC18:2 and 9:1 showed higher values (ca. 3 – 5%) than theoretical molecular weights, while LC16:4 had 6% less than the predicted value. This was attributed to the fact that the molecular weight of LA was higher than CL (114.14 and 144.13g/mole for CL and LA respectively [38, 39]). The degree of methacrylation was estimated by integration of the vinyl protons and normalized to the DEG protons at 3.6 ppm which remained unchanged in all variations. High methacrylation (above 85%) was crucial to ensure comparability among the synthesized LC scaffolds throughout the testing. Variation in the methacrylation could lead to less stable structures, more unsolidified residues in the material and open chain ends after photochemical vitrification. This would consequently affect the mechanical properties, cause

local acidification and fast degradation of the LC chains due to the lack of complete chain-end-capping with methacrylate groups [40].

For the estimation of the reactivity of the resulting three LC variants a photo-DSC equipped with a UV source was used, to get insights into the curing behavior of the material prior to the extensive TPP sample preparation (see Figure 6). Small values of the time to maximal heat generation t_{max} correspond to highly reactive photopolymers. Therefore the variants of reactivity in terms t_{max} were as follows LC 18:2<16:4<9:1 at 30°C.

High temperatures foster the curing process expressed by lower t_{max} values. As clearly shown in Figure 6, LC 18:2 was less reactive than LC 9:1 and LC 16:4 for all temperatures. This was consistent with the generated heat of polymerization. The lower initiation limit of the polymerization with the UV source used appeared to be at 8-9 s, including the time needed for the lamp to develop full power. LC 9:1 generated more heat due to the [molecular weight]:[methacryl-group] ratio, resulting in a higher double bond density which correlated with the higher ΔH values. The temperature dependency was most prominent in LC 9:1, resulting in large steps between 30°C and 70°C, with a change in ΔH of *ca.* 25 J/g, compared with a change of < 8 J/g for the other compositions. This could have been related to the higher amount of double bonds present and the accessibility of these with temperature (viscosity) [41].

For a deeper understanding and better comparison of the three materials, the absolute conversion was calculated Eq. (2) and (3) (Figure 7) [31, 32, 42]. A value of 100% corresponded to complete reaction of the double bonds during network formation upon irradiation; smaller values corresponded to partially unreacted double bonds and increasing unsolidified phase. The calculations of conversions revealed the high reactivity and large differences between temperatures for LC9:1, which are a result of its incomplete conversion at low temperatures (less than 70%). When rating the different compositions via their percentage of conversion at 30°C, they followed the order of LC 16:4> 18:2> 9:1. There was no significant difference in t_{max} of curing for LC9:1 at different temperatures, Figure 6. The conversion in LC9:1 appeared to be highly dependent on the temperature. At low temperature the conversion was the lowest of all precursors, an effect reversed at 70°C, a temperature at which the motility (molecule size) is a function of conversion. In general, all compositions had a potential for structuring using 2PP method [41].

Manufacturing of 3D scaffolds

The designated scaffolds were further analyzed after production in the TPP device to verify consistency of the stereo-lithography (STL) model file with SEM micrographs of the manufactured scaffolds (see Figure 8). SEM micrographs revealed a high similarity of structure and consistency with the applied model. The pore sizes for all LC scaffolds were *ca.* 300 µm and throat sizes varied from 152 µm (for LC9:1) to 177 µm (for LC16:4 and 18:2), see Table 3. Pore geometry deviated from spherical shape to ellipsoidal with aspect ratio of approximately 1.10 for the produced scaffolds. This was suggested to be due to shrinkage after solidification. Pore sizes were in the often quoted ideal range of 200-400 µm, which was supposed to facilitate osteo-differentiation and functional bone formation [12, 43, 44]. The translation of the STL model to the structure (see Figure 8) was very good and reproducible in terms of pores and throat sizes achieved (see Table 3).

SEM was also conducted for investigation of the scaffold microtopography. The surfaces of the scaffolds had a distinctive texture morphology (see Figure 8B – D), which provided roughness and hence could potentially improve cell adhesion. Error! Reference source not found.E revealed that the line to line distance was visible (13µm), creating room and possibilities for further modification to adhesion and cell preferences. The hatching distance of 13 µm was chosen to reduce the writing time and to form pits (~ 10µm) for physical cellular adhesion.

Scaffold Treatment

Since sterilisation is an essential prerequisite for medical devices before use, all the scaffolds were sterilised using gamma radiation at the standard dose of 25 ± 2.5 kGy [33, 45] and kept in sterilisation bags prior to use. Gamma radiation was preferred as a method of sterilisation due to its high efficiency, high penetration and negligible thermal effects [46]. However, gamma sterilisation is known to induce molecular changes for polymeric materials by chain scission and crosslinking [46-48]. Therefore, the effect of gamma sterilisation on LC scaffolds was also evaluated by compression testing prior to and post sterilisation as shown in Figure 9. No significant changes were observed in stress-strain curves for all LC16:4. 18:2 and 9:1 scaffolds post sterilisation. This was suggested to be due to the double effects of gamma irradiation, crosslinking and chain scission, as both have opposite impacts on molecular weight and mechanical properties of the polymers [46-48].

DSC traces for LC scaffolds can be seen in Figure 10. The glass transition temperatures (T_g) for LC16:4, 18:2 and 9:1 were 4.8, 31 and 33 ºC respectively as reported in Table 1. Endothermic peaks were also observed at 281ºC for LC16:4 and 365ºC (see Table **4**) for LC18:2 and 9:1, and represented decomposition temperature (T_d). These peaks were suggested to be due to thermal decomposition of the PLCL copolymers. Values of T_g and T_d for LC18:2 and 9:1were similar, whilst LC16:4 showed significantly lower results, which was ascribed to the variation in D,L lactide ratio to ε-caprolactone to (LA/CL) ratio in different scaffolds [49, 50] (see Table 2). No melting peaks were detected for any of the scaffolds, possibly due to the high crosslinking in the photo-polymerisation process.

Degradation and mechanical properties

Figure 11 A, B and C show changes in weight, mass loss and pH of LC16:4, 18:2 and 9:1 scaffolds versus time throughout degradation in PBS at different temperatures of 37, 50 and 65ºC. Initial increases were seen in the wet weight of LC16:4, 18:2 and 9:1 scaffolds respectively up to 5 (at 37ºC) and 2 days at 50 and 65ºC, followed by stabilisation in weights of all scaffolds. The initial increase was attributed to fast water uptake till specimens attained saturation. LC16:4, 18:2 and 9:1 scaffolds maintained their weight change at ~2, 2.5 and 5% for the duration of the study at 37ºC. This plateau in wet weight of the scaffolds was a result of the balance between water uptake and mass loss [27]. In contrast, a second phase of increase in the scaffold weights was seen after 25 and 6 days of degradation at 50 and 65ºC respectively, which was a consequence of imbalance between water uptake and mass loss (i.e. mass loss due to hydrolytic degradation became dominant) [27].

From Figure 11 D, E and F, the percentage change in mass loss for the scaffolds can be seen versus degradation time at different temperatures. Mass loss for LC16:4, 18:2 and 9:1 scaffolds showed a gradual increase of degradation time at different temperatures. This was attributed to continuous degradation of the scaffold materials. The relation between percentage of mass loss for all scaffolds and degradation time at 37, 50 and 65ºC followed a linear function with regression coefficient greater than 0.98. Moreover, the rate of mass loss for each scaffold type, determined as the gradient of absolute mass loss vs time, increased as degradation temperature changed from 37ºC to 65ºC. Rates of mass loss of LC16:4 scaffolds at 37, 50 and 65ºC were lower than that for LC18:2 and 9:1. This could be ascribed to the variation in LA/CL ratio

between LC16:4, 18:2 and 9:1 scaffold materials (see LA: D,L-lactide, CL: ε-Caprolactone, TEA: trimethylamine and MACL: methacryloyl chloride

Table **2** and Figure 5). It was reported that the required time for complete resorption (degradation time) of poly(D,L-lactide) (PDLLA) is approximately 1-2 years, whilst poly(ε-caprolactone) (PCL) requires 2-4 years [1, 51, 52]. Consequently, it was expected that an increase in CL content would lead to a lower degradation rate. LC16:4 scaffolds had the highest amount of CL compared to LC18:2 and 9:1 consistent with their low weight change and mass loss over the degradation in PBS at different temperatures.

The degradation medium (PBS) remained at neutral pH of 7.3 ± 0.1 for all scaffolds during degradation at 37 and 50ºC due to buffering capability of PBS (see Figure 11 G and H). At 65ºC, pH of PBS for LC18:2 and 9:1 scaffolds decreased to be around 7.0 after 6 days (see Figure 11 I) as a result of faster release of acidic degradation by-products of poly(L-lactide-co-ε-caprolactone).

Calculation of activation energy

The rate of mass loss change for the scaffolds yielded an Arrhenius relationship with regression coefficients greater than 99% (see Figure 12). The degradation activation energies obtained were 87.9, 82.7 and 94.9 kJ mol^{-1} for LC16:4, LC18:2 and LC9:1 respectively. Arrhenius relation has been conducted for the change in several parameters of biodegradable polymers such as molecular weight, breaking strength, viscosity and mass loss [23, 27, 35, 53, 54]. The majority of previous publications used change in molecular weight over degradation time at different temperatures. However, it was not applicable to measure the molecular weight for photo cross-linked copolymers using gel permeation chromatography (GPC) due to their insolubility in organic solvents. Therefore, the change in rate of mass loss at different temperatures was used in this study to calculate the degradation activation energy. Weir *et al.*[35] and Agrawal *et al.*[53] determined activation energies for 50%PLA-50%PGA copolymer and PLLA (113.9 and 100.5 kJ mol^{-1}) through the change in molecular weight against degradation temperature. Degradation activation energy was also determined for 10%PLLA–90%PGA through change in tensile breaking strength during degradation at different temperatures [29]. The activation energy ranged between 95.9 kJ mol^{-1} and 102.6 kJ mol^{-1}. Pietrzak *et al.*[23] applied the Arrhenius equation to

change in inherent viscosity for a 82%PLLA-18%PGA copolymer and obtained an activation energy of 100.1 kJ mol^{-1}. Previous studies have suggested that degradation activation energies were independent of the geometry and composition of the PLLA-PGA copolymers. The values of activation energy obtained for LC scaffolds using rate of mass loss were similar to the published results for biodegradable polymers [23, 29, 53].

Prediction of long-term effects

A correlation between a long-term degradation study at 37ºC and short studies at elevated temperatures (50 and 65ºC) was conducted in order to make a prediction for degradation time, using a similar procedure to that presented by Litherland *et al.*[55]. By fitting plots relating half-life of mass loss (Time ($M_{1/2}$)), required time for the scaffold to lose 50% of their initial weight, to degradation temperature, a power equation were obtained (see Figure 13) and regression coefficients were greater than 0.99. Therefore, the degradation rate of the scaffolds at other degradation temperatures could be anticipated through the obtained fitting equations.

The changes in compressive modulus and strength of LC16:4, 18:2 and 9:1 scaffolds against time during degradation in PBS at 37ºC are shown in Figure 14. Before degradation, compressive moduli were *ca.* 0.27, 2 and 4 MPa for LC16:4, 18:2 and 9:2 respectively. Compressive strengths at 20% strain for LC18:2 and 9:1 (0.2 and 0.55 MPa) scaffolds were also significantly higher ($P<0.001$) than LCM3 (0.05MPa). Mechanical properties of these scaffolds were mainly dependent on their material composition (i.e. LA/CL ratio) as all scaffolds have almost the same porosity and pore sizes. Young's modulus for poly(D,L-lactide) is approximately five times higher than poly(ε-caprolactone) alone [51, 52]. Therefore, mechanical properties of the copolymer would be expected to decrease as the CL content increased as shown in Figure 14. Similar findings were published for poly(L-lactide-co-ε-caprolactone) copolymers by Fernandez et al. [50]. Tensile modulus and strength of the copolymer films decreased from 1343 to 12MPa and from 26.6 to 17.2 MPa respectively as the CL contents increased from 10 to 30%. No significant changes ($P>0.05$) were seen in both strength and modulus for all scaffolds over 20 days of degradation in PBS at 37ºC. After this period all scaffolds showed decreases in strength and modulus till end of the study at 83 days. The large errors for LC18:2 and 9:1 scaffolds were due to the mechanical testing temperature (25±1ºC) which unfortunately was close to the onset glass transition temperature for LC18:2 and 9:1 (~23.7±0.7ºC) as reported in Table **4**. The onset glass transition for LC16:4 scaffolds (-1.6 ± 1ºC) was significantly lower than the testing

temperature and this explained the lower variation in results showing a smooth and gradual decrease in their compressive modulus and strength properties (inset, Figure 14 A and B). Reduction in compressive properties for all scaffolds over time was ascribed to continuous degradation of the scaffold materials as can be seen from variations in mass loss against time (see Figure 11 D).

Temperature and strain conditions (25ºC and 20% respectively) of compressive testing were chosen to fit the surgical environment and handling procedures. Temperature of the surgery theatre is usually fixed at 25ºC and the surgeon is anticipated to compress the scaffold up to 20% before implantation in order to obviate scaffold dislocation.

Optical images were captured for LC scaffolds (see Figure 15) to investigate the macroscopic changes throughout the degradation processes at different temperatures (37, 50 and 65ºC). For LC16:4 scaffolds, no significant changes were detected at different time points and temperatures. Conversely, large deteriorations were observed for LC18:2 and 9:1 scaffolds in particular at elevated temperatures. This was due to two reasons; fast degradation rates and thermal effects. Repeatable heating-cooling cycles during degradation at 37ºC and testing or changing PBS at room temperature (~20ºC) were suggested to accelerate the degradation rate of the scaffolds (thermal effect). Effects of heating-cooling cycles were more significant on LC18:2 and 9:1 than LC16:4 due to their thermal properties (see Table **4**). Heating-cooling cycles covered a range of temperatures (37ºC – 20ºC) which was around their glass transition temperature for LC18:2 and 9:1 scaffolds, whilst T_g of LC16:4 was out of this range.

Conclusion:

3D porous scaffolds were manufactured via a 2PP polymerisation technology based on a Schwarz Primitive minimal surface derived unit cells with µm resolution and pore size of about 300 µm. For commercialization, the writing time is still the main limitation for manufacturing scaffolds in millimeter dimensions with micrometer resolutions using 2PP technology. 2PP enabled production of well-defined microstructures with good reproducibility, which was crucial for future biological analyses. Changes in thermal, degradation and mechanical properties of all scaffolds were related to their chemical composition (LA/CL ratio) and accelerated degradation was predictable as the rate of mass loss for all scaffolds increased gradually by increasing degradation temperature from 37 to 65ºC. The activation energies for degradation were

independent of chain length and composition. By applying a temperature superposition, a feasible accelerated method was generated to predict long-term degradation time for LC scaffolds at 37ºC. These materials have the potential to replace state-of-the-art implants and allografts as they can offer slower degradation and softer mechanics and avoid the acidity-burst at degradation compared to LA, and they will be translated into biological testing to determine the effect of CL on osteogenesis.

Acknowledgements:

This research project has received funding from the European Union's Seventh Framework Programme (FP7/2007-2013) under grant agreement n. 263363

References:

1. Woodruff, M.A. and D.W. Hutmacher, *The return of a forgotten polymer—Polycaprolactone in the 21st century.* Progress in Polymer Science, 2010. **35**(10): p. 1217-1256.

2. Woodruff, M.A., et al., *Bone tissue engineering: from bench to bedside.* Materials Today, 2012. **15**(10): p. 430-435.

3. Ulery, B.D., L.S. Nair, and C.T. Laurencin, *Biomedical applications of biodegradable polymers.* Journal of Polymer Science Part B: Polymer Physics, 2011. **49**(12): p. 832-864.

4. Yang, X.B., et al., *Biomimetic collagen scaffolds for human bone cell growth and differentiation.* Tissue Eng, 2004. **10**(7-8): p. 1148-59.

5. Ho, M.-H., et al., *Preparation of porous scaffolds by using freeze-extraction and freeze-gelation methods.* Biomaterials, 2004. **25**(1): p. 129-138.

6. Lannutti, J., et al., *Electrospinning for tissue engineering scaffolds.* Materials Science and Engineering C, 2007. **27**(3): p. 504-509.

7. Brown, T.D., et al., *Melt electrospinning of poly(epsilon-caprolactone) scaffolds: phenomenological observations associated with collection and direct writing.* Materials science & engineering. C, Materials for biological applications, 2014. **45**: p. 698-708.

8. Brown, T.D., P.D. Dalton, and D.W. Hutmacher, *Direct writing by way of melt electrospinning.* Advanced Materials, 2011. **23**(47): p. 5651-7.

9. Zhu, J., *Bioactive modification of poly(ethylene glycol) hydrogels for tissue engineering.* Biomaterials, 2010. **31**(17): p. 4639-56.

10. Lutolf, M.P. and J.A. Hubbell, *Synthetic biomaterials as instructive extracellular microenvironments for morphogenesis in tissue engineering.* Nature biotechnology, 2005. **23**(1): p. 47-55.

11. Tsang, V.L. and S.N. Bhatia, *Three-dimensional tissue fabrication.* Advanced drug delivery reviews, 2004. **56**(11): p. 1635-47.

12. Tse, J.R. and A.J. Engler, *Preparation of hydrogel substrates with tunable mechanical properties.* Current protocols in cell biology / editorial board, Juan S. Bonifacino ... [et al.], 2010. **Chapter 10**: p. Unit 10 16.

13. Hutmacher, D.W., *Scaffolds in tissue engineering bone and cartilage.* Biomaterials, 2000. **21**: p. 2529-2543.

14. Landers, R., et al., *Rapid prototyping of scaffolds derived from thermoreversible hydrogels and tailored for applications in tissue engineering.* Biomaterials, 2002. **23**(23): p. 4437-47.

15. Rentsch, B., et al., *Embroidered and surface coated polycaprolactone-co-lactide scaffolds: a potential graft for bone tissue engineering.* Biomatter, 2012. **2**(3): p. 158-65.

16. Stampfl, J., et al., *Photopolymers with tunable mechanical properties processed by laser-based high-resolution stereolithography.* Journal of Micromechanics and Microengineering, 2008. **18**(12): p. 125014.

17. Göppert-Mayer, M., *Elementary processes with two quantum transitions.* Annalen der Physik, 2009. **18**: p. 466-479.

18. Galajda, P. and P. Ormos, *Complex micromachines produced and driven by light.* Applied Physics Letters, 2001. **78**: p. 249-251.

19. Kawata, S., et al., *Finer features for functional microdevices.* Nature, 2001. **412**: p. 697-698.

20. Weiß, T., et al., *Two-Photon Polymerization of Biocompatible Photopolymers for Microstructured 3D Biointerfaces.* Advanced Engineering Materials, 2011. **13**(9): p. B264-B273.

21. Berg, A., et al., *Synthesis of photopolymerizable hydrophilic macromers and evaluation of their applicability as reactive resin components for the fabrication of three-dimensionally structured hydrogel matrices by 2-photon-polymerization.* Advanced Engineering Materials, 2011. **13**: p. B274-B284.

22. WeissŸ, T., et al., *Two-Photon polymerization for microfabrication of three-dimensional scaffolds for tissue engineering application.* Engineering in Life Sciences, 2009. **9**(5): p. 384-390.

23. Pietrzak, W.S., M. Kumar, and B.L. Eppley, *The Influence of Temperature on the Degradation Rate of LactoSorb Copolymer.* Journal of Craniofacial Surgery, 2003. **14**(2): p. 176-183.

24. Lam, C.X., et al., *Dynamics of in vitro polymer degradation of polycaprolactone-based scaffolds: accelerated versus simulated physiological conditions.* Biomed Mater, 2008. **3**(3): p. 034108.

25. Lee, S.-H., J. Lee, and Y.-S. Cho, *Analysis of degradation rate for dimensionless surface area of well-interconnected PCL scaffold via in-vitro accelerated degradation experiment.* Tissue Engineering and Regenerative Medicine, 2014. **11**(6): p. 446-452.

26. Lyu, et al., *Kinetics and Time-Temperature Equivalence of Polymer Degradation.* Biomacromolecules, 2007. **8**(7): p. 2301-2310.

27. Felfel, R.M., et al., *Accelerated in vitro degradation properties of polylactic acid/phosphate glass fibre composites.* Journal of Materials Science, 2015. **50**(11): p. 3942-3955.

28. Claes, L.E., et al., *New bioresorbable pin for the reduction of small bony fragments: design, mechanical properties and in vitro degradation.* Biomaterials, 1996. **17**(16): p. 1621-1626.

29. Deng, M., et al., *Effect of load and temperature on in vitro degradation of poly(glycolide-co-L-lactide) multifilament braids.* Biomaterials, 2005. **26**(20): p. 4327-4336.

30. Davis, K.A., J.A. Burdick, and K.S. Anseth, *Photoinitiated crosslinked degradable copolymer networks for tissue engineering applications.* Biomaterials, 2003. **24**: p. 2485-2495.

31. Wu, K.C. and J.W. Halloran, *Photopolymerization monitoring of ceramic stereolithography resins by FTIR methods.* Journal of Material Science, 2005. **40**: p. 71-76.

32. Lovestead, T.M., et al., *Understanding multivinyl monomer photopolymerization kinetics through modeling and GPC investigation of degradable networks.* Polymer, 2005. **46**(16): p. 6226-6234.

33. *BS EN ISO 11137-2 (2013) Sterilization of health care products. Radiation. Establishing the sterilization dose*

34. 10993-13, B.E.I., in *Biological evaluation of medical devices. Identification and quantification of degradation products from polymeric medical devices* 2010.

35. Weir, N., et al., *Degradation of poly-L-lactide. Part 2: increased temperature accelerated degradation.* Proceedings of the Institution of Mechanical Engineers, Part H: Journal of Engineering in Medicine, 2004. **218**(5): p. 321-330.

36. Weir, N., et al., *Degradation of poly-L-lactide. Part 1: in vitro and in vivo physiological temperature degradation.* Proceedings of the Institution of Mechanical Engineers, Part H: Journal of Engineering in Medicine, 2004. **218**(5): p. 307-319.

37. *ASTM D1621 - 10 (2010), Standard Test Method for Compressive Properties of Rigid Cellular Plastics*.

38. Li, C.-Y., D.-C. Liu, and B.-T. Ko, *Synthesis, characterization and reactivity of single-site aluminium amides bearing benzotriazole phenoxide ligands: catalysis for ring-opening polymerization of lactide and carbon dioxide/propylene oxide coupling.* Dalton Transactions, 2013. **42**(32): p. 11488-11496.

39. Heijkants, R.G.J.C., et al., *Extruder synthesis of a new class of polyurethanes: Polyacylurethanes based on poly(ε-caprolactone) oligomers.* Polymer, 2005. **46**(21): p. 8981-8989.

40. Burdick, J.A., et al., *An initial investigation of photocurable three-dimensional lactic acid based scaffolds in a critical-sized cranial defect.* Biomaterials, 2003. **24**(9): p. 1613-20.

41. Tobita, H., *Molecular weight distribution formed through chain-length-dependent crosslinking reactions.* Macromolecular Theory and Simulations, 1998. **7**: p. 225-232.

42. Ye, Q., et al., *Relationship of solvent to the photopolymerization process, properties, and structure in model dentin adhesives.* Journal of biomedical materials research. Part A, 2007. **80**(2): p. 342-50.

43. Papaioannou, T.G., et al., *Assessment of vascular wall shear stress and implications for atherosclerotic disease.* International journal of cardiology, 2006. **113**(1): p. 12-8.

44. Papaioannou, T.G. and C. Stefanadis, *Vascular wall shear stress: basic principles and methods.* Hellenic journal of cardiology : HJC = Hellenike kardiologike epitheorese, 2005. **46**(1): p. 9-15.

45. Kowalski, J.B., Y. Aoshuang, and A. Tallentire, *Radiation sterilization — evaluation of a new approach for substantiation of 25 kGy.* Radiation Physics and Chemistry, 2000. **58**(1): p. 77-86.

46. Cottam, E., et al., *Effect of sterilisation by gamma irradiation on the ability of polycaprolactone (PCL) to act as a scaffold material.* Medical Engineering & Physics, 2009. **31**(2): p. 221-226.

47. Narkis, M., et al., *Irradiation effects on polycaprolactone.* Polymer, 1985. **26**(1): p. 50-54.

48. Augustine, R., et al., *Dose-Dependent Effects of Gamma Irradiation on the Materials Properties and Cell Proliferation of Electrospun Polycaprolactone Tissue Engineering Scaffolds.* International Journal of Polymeric Materials and Polymeric Biomaterials, 2015. **64**(10): p. 526-533.

49. Fernández, J., et al., *A new generation of poly(lactide/ε-caprolactone) polymeric biomaterials for application in the medical field.* Journal of Biomedical Materials Research Part A, 2013. **102**(10): p. 3573–3584.

50. Fernández, J., A. Etxeberria, and J.-R. Sarasua, *Synthesis, structure and properties of poly(L-lactide-co--caprolactone) statistical copolymers.* Journal of the Mechanical Behavior of Biomedical Materials, 2012. **9**(0): p. 100-112.

51. Middleton, J.C. and A.J. Tipton, *Synthetic biodegradable polymers as orthopedic devices.* Biomaterials, 2000. **21**(23): p. 2335-2346.

52. Maurus, P.B. and C.C. Kaeding, *Bioabsorbable implant material review.* Operative Techniques in Sports Medicine, 2004. **12**(3): p. 158-160.

53. Agrawal, C.M., et al., *Elevated Temperature Degradation of a 50:50 Copolymer of PLA-PGA.* Tissue Engineering, 1997. **3**(4): p. 345-352.

54. Deng, M., et al., *A study on in vitro degradation behavior of a poly(glycolide-co-l-lactide) monofilament.* Acta Biomaterialia, 2008. **4**(5): p. 1382-1391.

55. Litherland, K.L., D.R. Oakley, and B.A. Proctor, *The use of accelerated ageing procedures to predict the long term strength of GRC composites.* Cement and Concrete Research, 1981. **11**(3): p. 455-466.

Tables:

Table 1: Experimental details for LC synthesis. DEG amount remained constant.

	LA		CL		TEA		MACL	
	m [g]	n [mmol]	m [g]	n [mmol]	m [g]	n [mmol]	m [g]	n [mmol]
LC16:4	18.90	131.13	7.65	67.02	4.71	46.54	4.33	41.42
LC18:2	23.63	163.95	3.83	33.55	4.71	46.54	4.33	41.42
LC9:1	11.82	81.97	1.92	16.78	5.11	50.50	4.84	46.32

LA: D,L-lactide, CL: ε-Caprolactone, TEA: trimethylamine and MACL: methacryloyl chloride

Table 2: Results obtained from 1H-NMR analysis.

	LC 9:1	LC 16:4	LC 18:2
Lactide units	9,6	14,6	19
Caprolactone units	1.3	4.1	2.0
Molecular weight [g/mol]	1059	1742	1822
Theoretical (100% yield)	1005	1852	1768
Methacrylation [%]	89.5	88.1	87.4

Table 3: Dimensions of pores, pore throats and aspect ratios of LC scaffolds measured from SEM micrographs.

Scaffold type	Pore size (μm)	Throat size (μm)	Pore aspect ratio
LC16:4	314± 14	177±7	1.07±0.03
LC18:2	328±26	177±10	1.10±0.05
LC9:1	290±25	152±7	1.2±0.05

Table 4: Transition temperatures for LC scaffolds; onset glass transition, midpoint glass transition (T_g) and decomposition temperature (T_d).

Scaffold type	T_g (onset) ^oC	T_g (midpoint) ^oC	T_d ^oC
LC16:4	-1.6 ± 1	4.8 ± 0.1	281 ± 1
LC18:2	23.8 ± 0.7	31 ± 1.5	365 ± 2
LC9:1	23.7 ± 0.7	33 ± 0.5	365 ± 0.5

Figures:

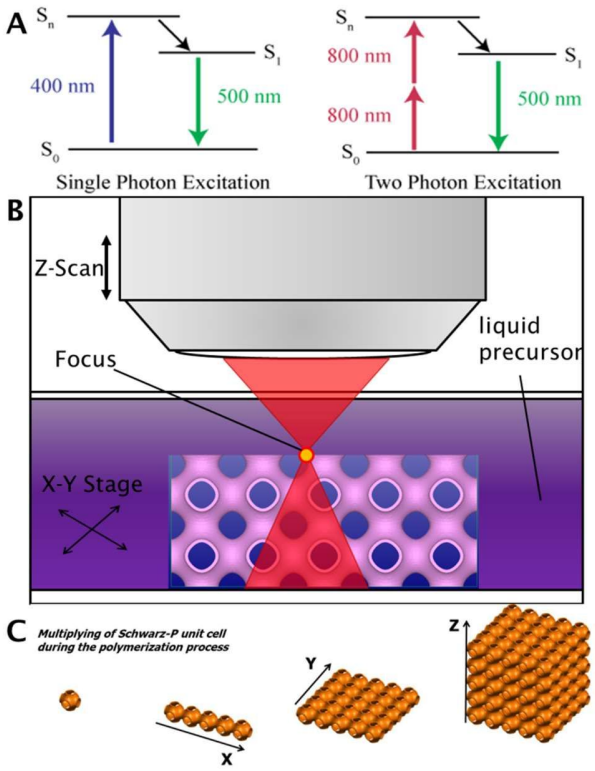

Figure 1: Generation of scaffolds using TPA. A: Term scheme of single-photon and two-photon excitation. B: Scheme of the TPP process. The laser beam is focused to high energies through an object lens. Through regulation of the parameters (power, speed, PI concentration) the energy necessary for polymerization is only given in the focus of the laser. By combining the Z-axis of the objective with a three-axis translation stage, structures can be built into three dimensions. C: Schwarz P scaffolds are built as arrays of unit cells (UC; 500µm) according to a matrix (e.g. 4x8x4 UC for the 2x4x2 mm^3 scaffolds) of coordinates with distances of one UC minus a calculated overlap.

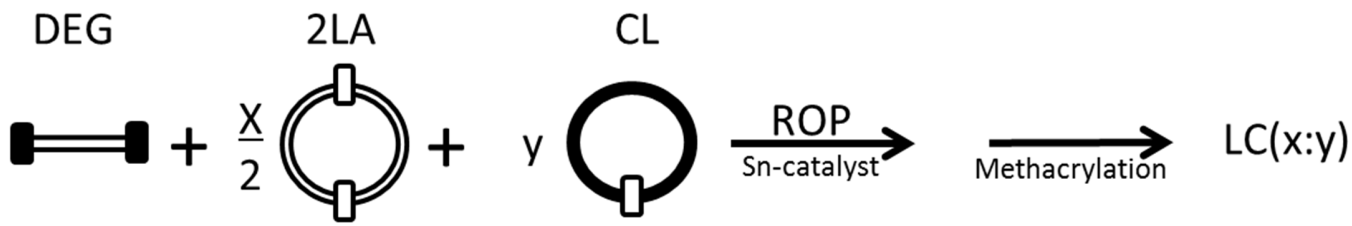

Figure 2: Reaction scheme of the ring-opening-polymerization (ROP) of the LC precursors.

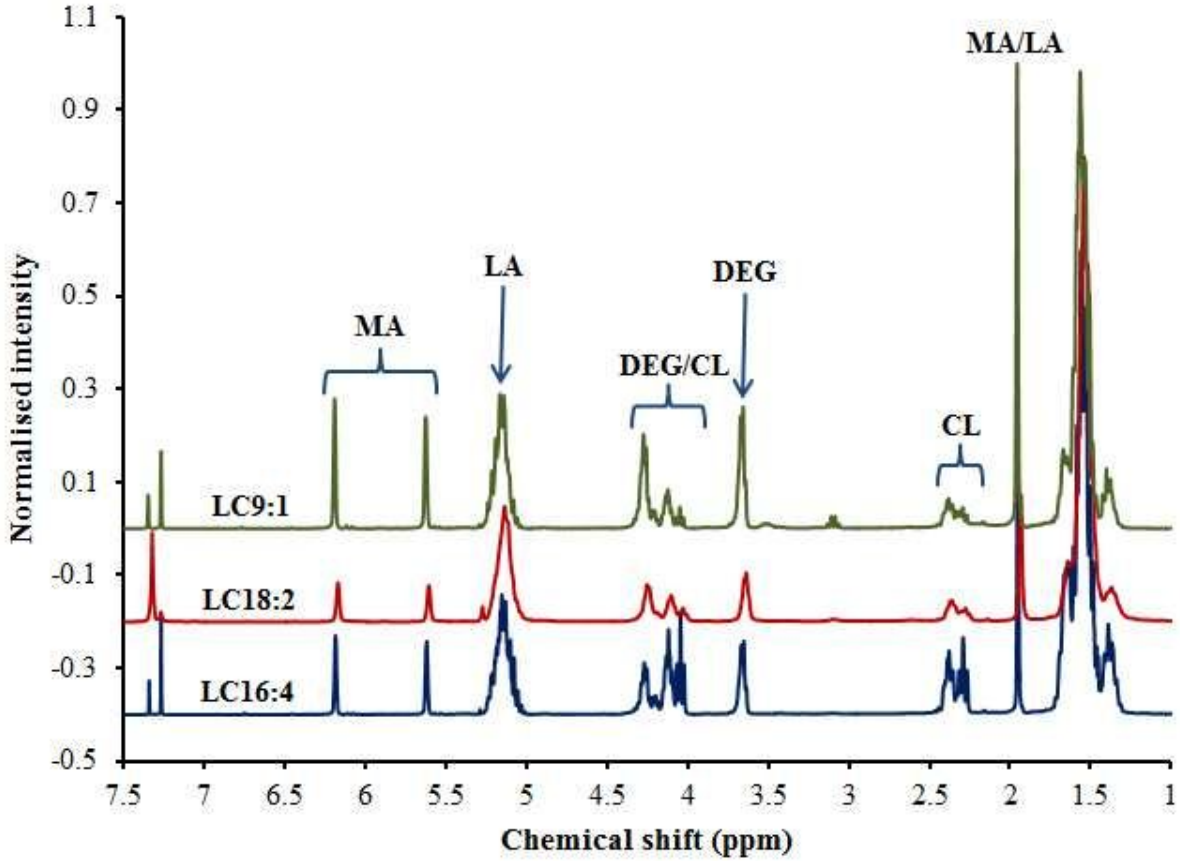

Figure 3: H-NMR spectra of the synthesized materials. The variation is most prominent in the CL signal at 2.5 ppm. DEG: Diethylenglycol, MA: Methacrylate group, CL: Caprolactone, LA: Lactide.

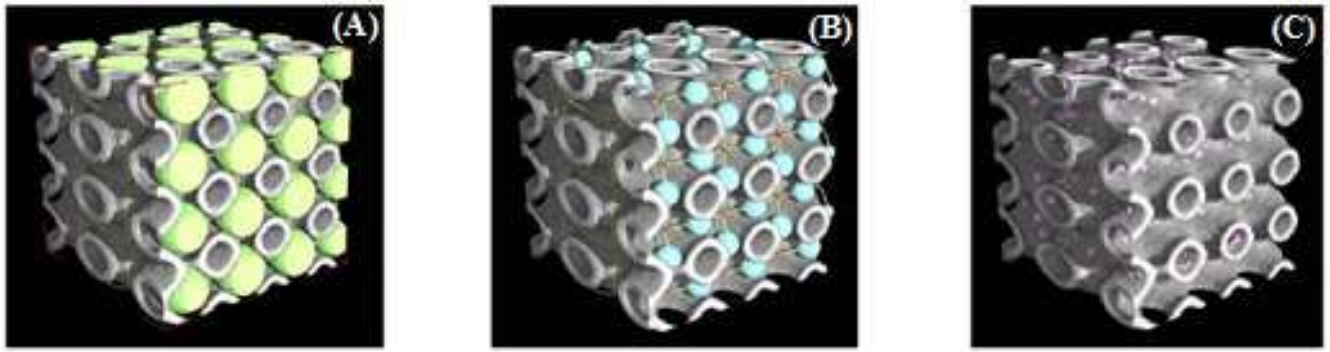

Figure 4: Scheme of the modulation sizing (8mm³) the pores by fitting maximised balls into it. Superposition of the maximal inscribed spheres used for the characterization of; A) pores, B) throats (size of interconnects) and C) walls (partial superposition with transparency).

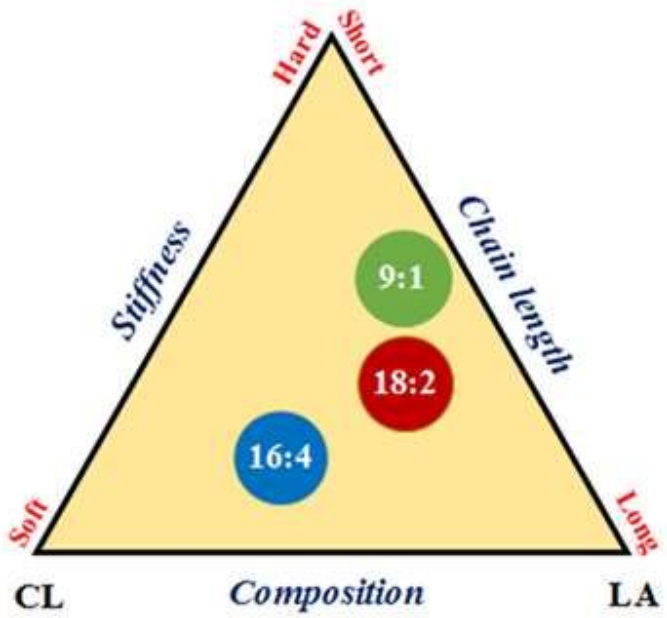

Figure 5: Schematic diagram showing change in stiffness and chain length for LC scaffolds due to difference in ε-caprolactone to D,L lactide ratio (CL:LA); 16:4, 18:2 and 9:1.

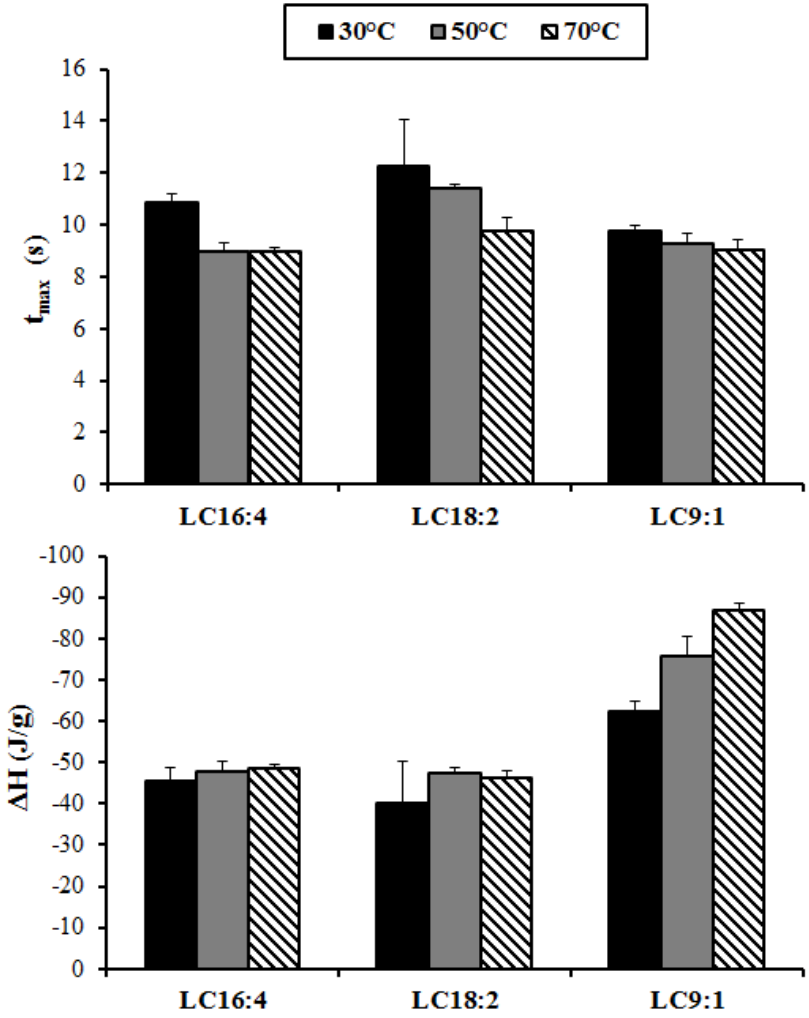

Figure 6: Results of photo-DSC curing experiments. Top: Time of maximal heat generation (tmax) of the LC variation at three different temperatures. Bottom: integrated total heat of reaction (ΔHsample (t)).

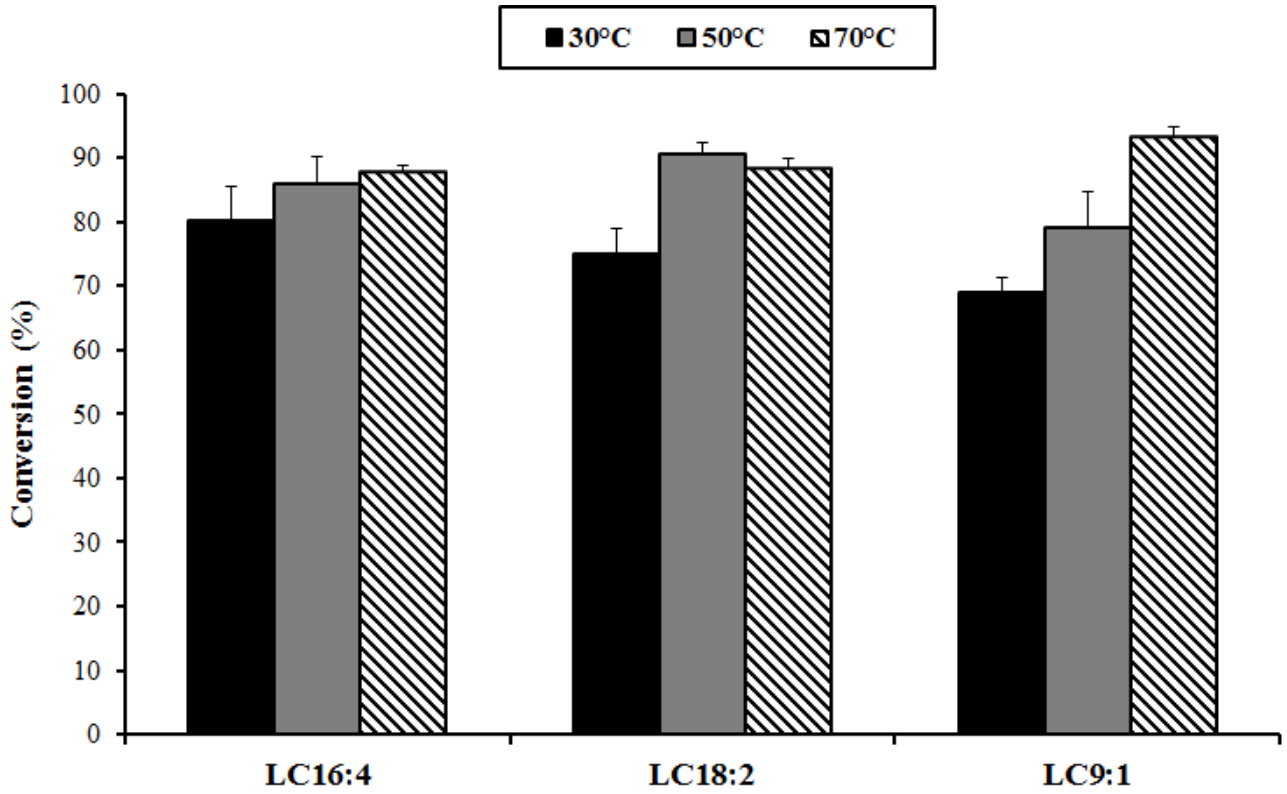

Figure 7: Absolute conversion of methacrylate groups in LC variants at different temperatures measured by DSC.

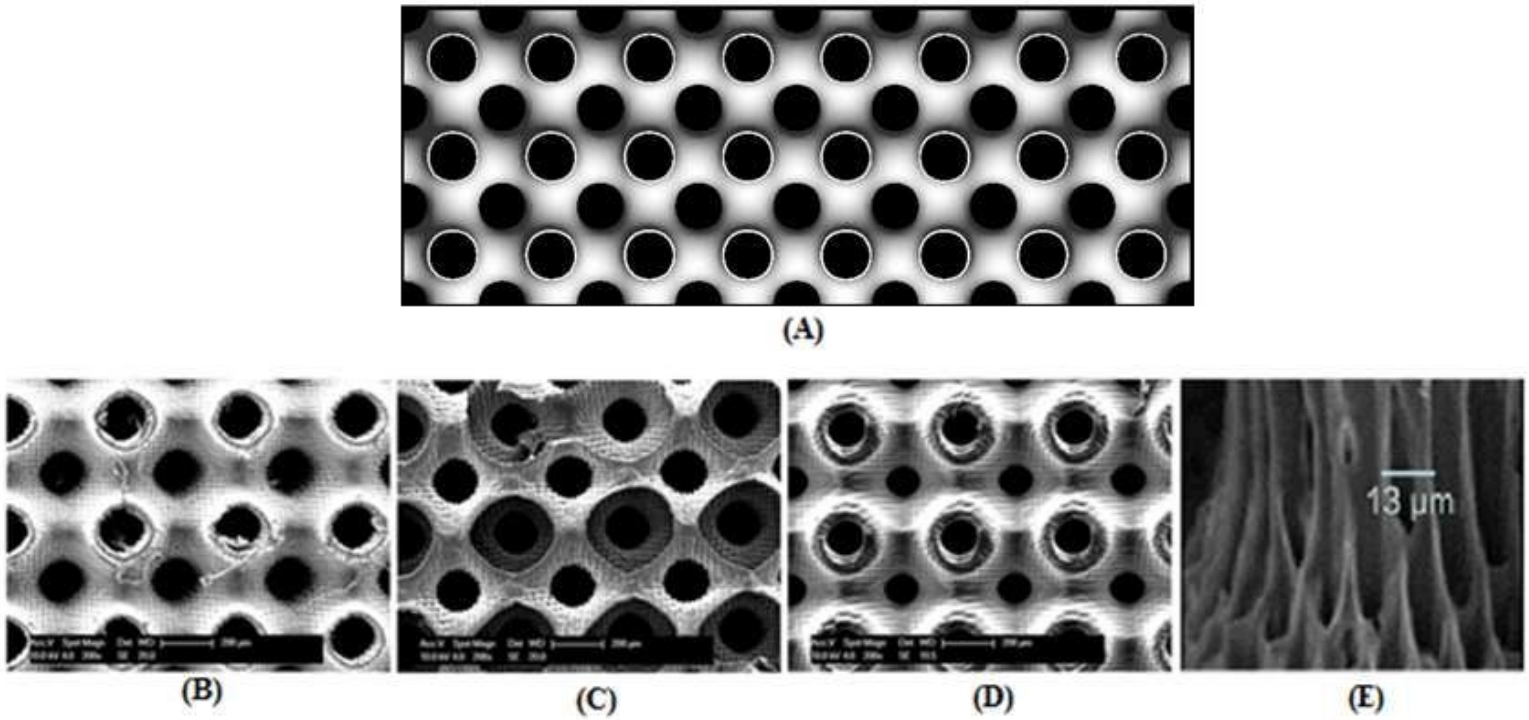

Figure 8: Translation from model to structure; (A) the input STL file, (B), (C) and (D) are SEM micrographs for top surface of LC16:4, LC18:2 and LC9:1 scaffolds respectively. (E) SEM micrograph of Schwarz P scaffold revealing the 13 µm hatch of the writing process.

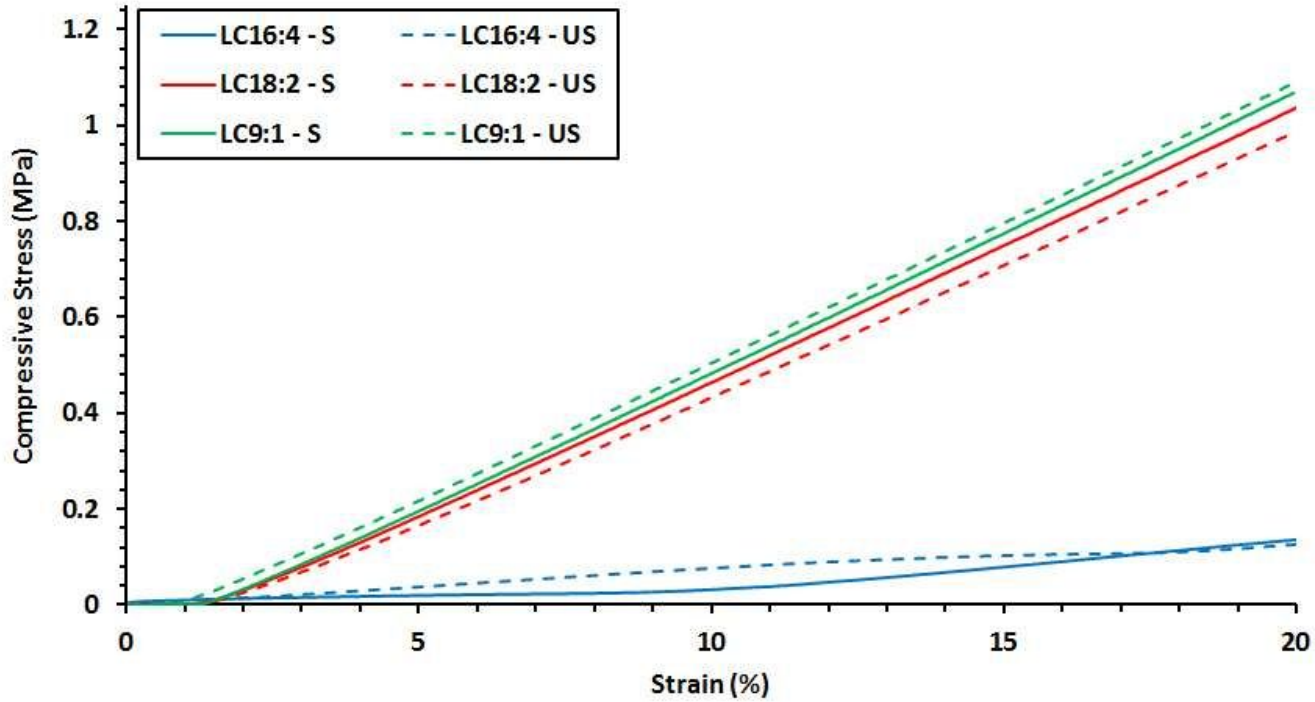

Figure 9: Compressive stress-strain curves up to 20% strain for LC scaffolds prior to and post gamma sterilisation at the dose of 25±2.5 kGy. S and US refer to sterilised and unsterilised specimens. Three samples (N=3) of each composition were tested and the average was used in this graph.

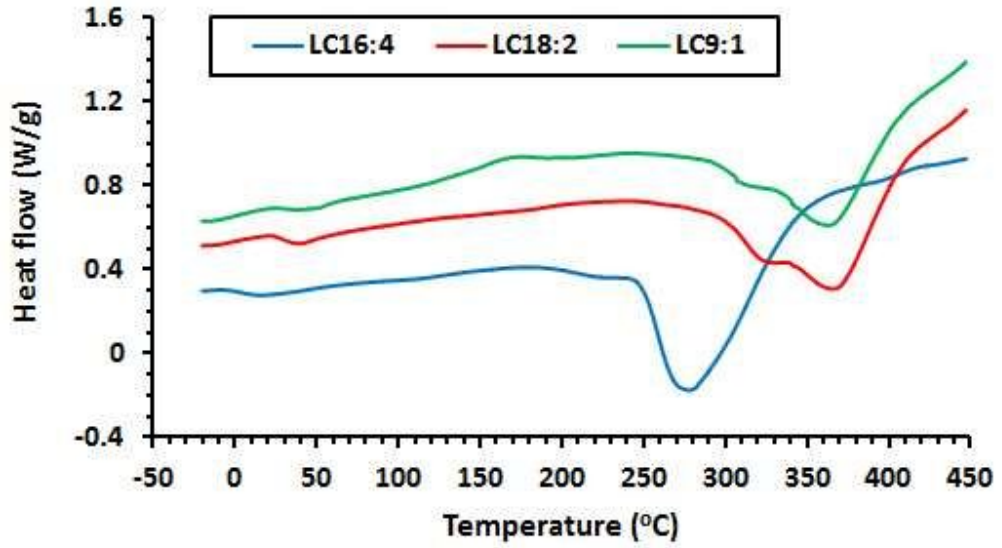

Figure 10: DSC thermograms for LC16:4, LC18:2 and LC9:1 scaffolds.

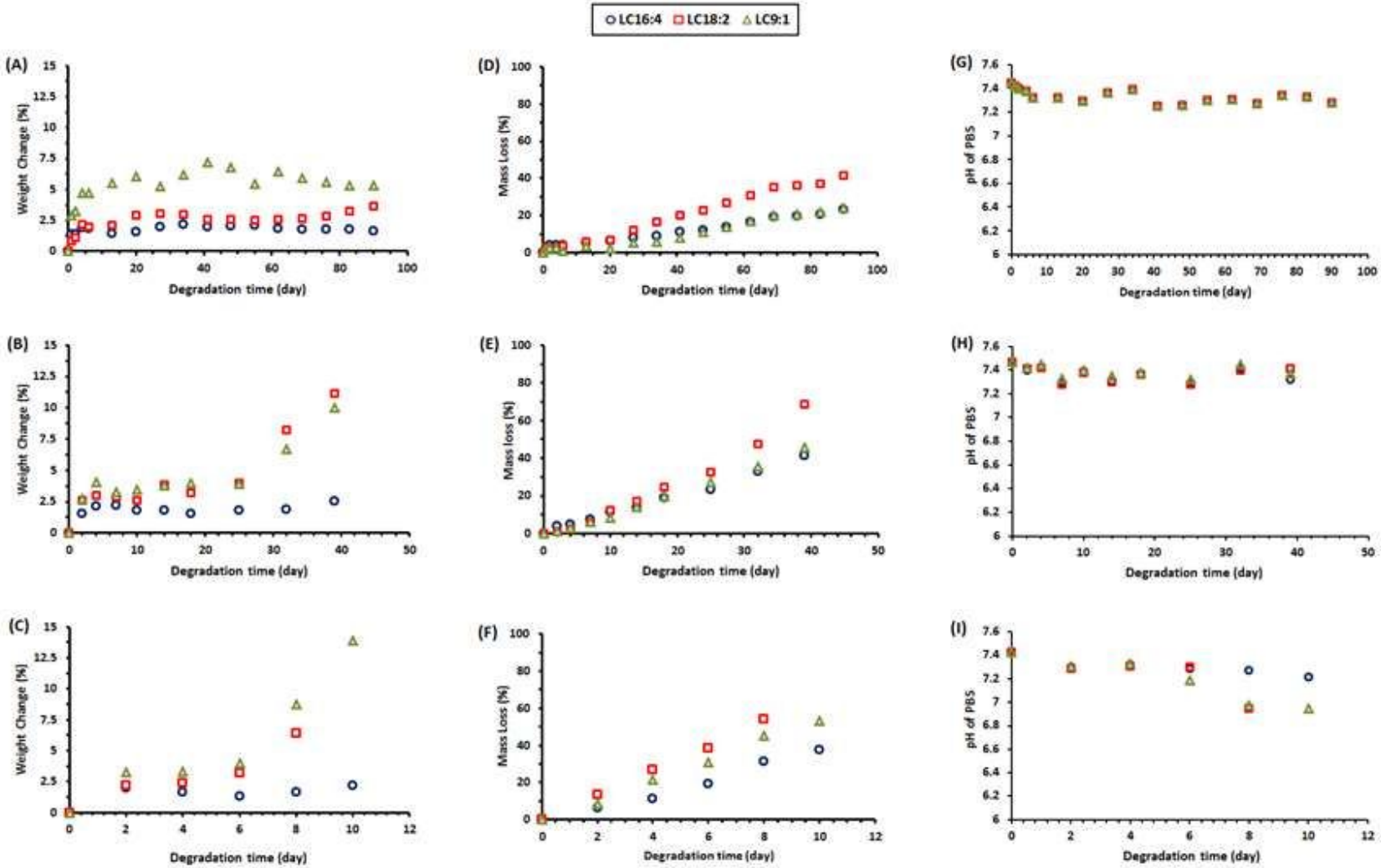

Figure 11: Change in wet weight (A, B and C), mass loss (D, E and F) and pH of degradation media (G, H and I) versus time for LC scaffolds during degradation in PBS at different temperature 37ºC (top row), 50ºC (middle row) and 65ºC (lower row). Changes in weight and mass were represented as a percentage value, while pH referred to the actual value.

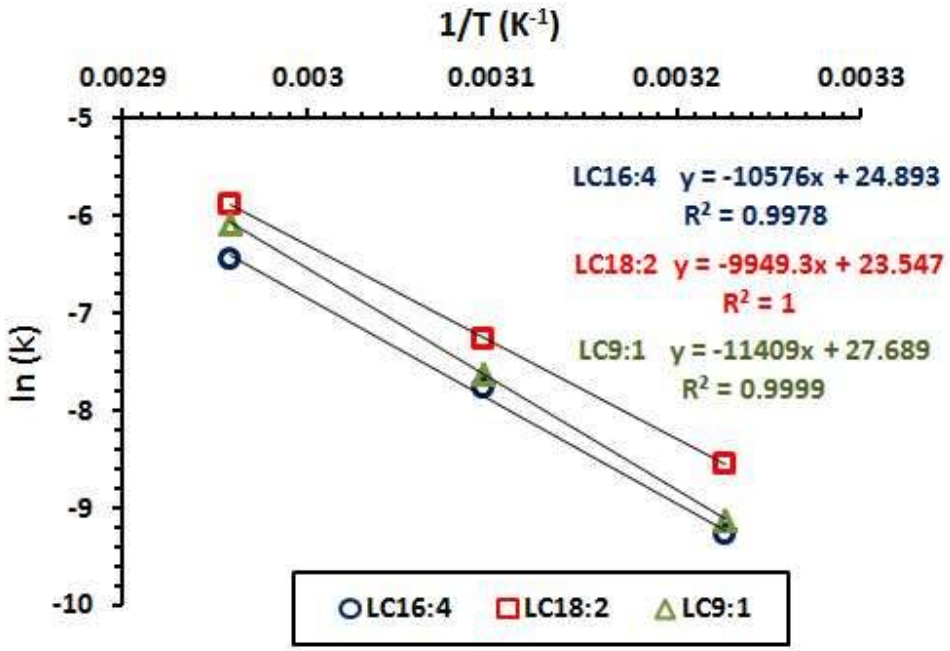

Figure 12: Arrhenius relation for the logarithm of rate of mass loss against inverse temperature in kelvin for LC scaffolds during degradation in PBS at different temperatures (37, 50 and 65oC).

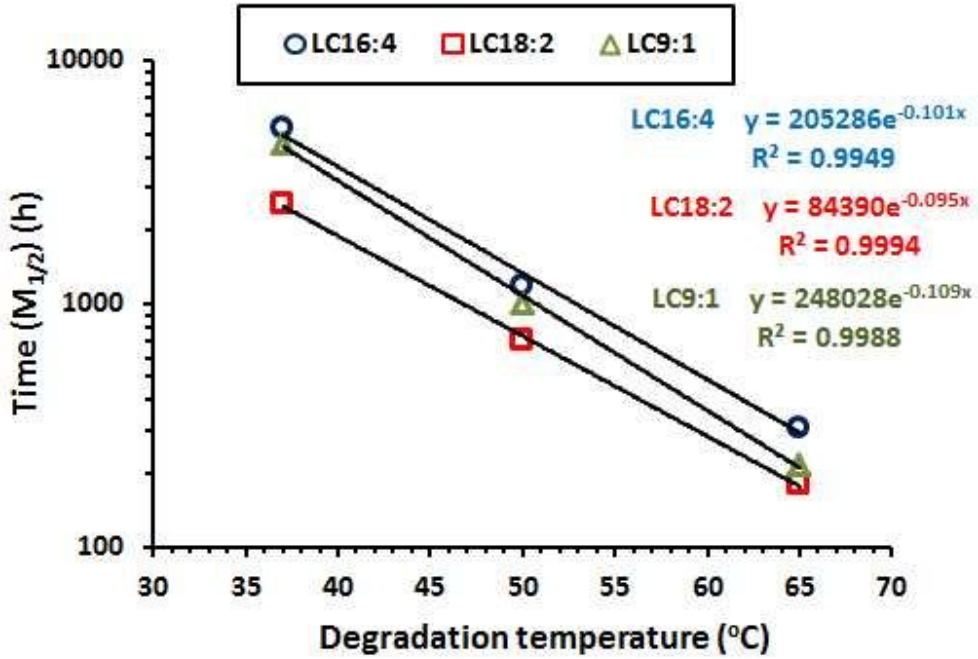

Figure 13: Half-life of LC scaffolds mass loss (i.e. required time for the scaffolds to lose 50% of their initial weight) versus degradation temperature during degradation in PBS at different temperatures

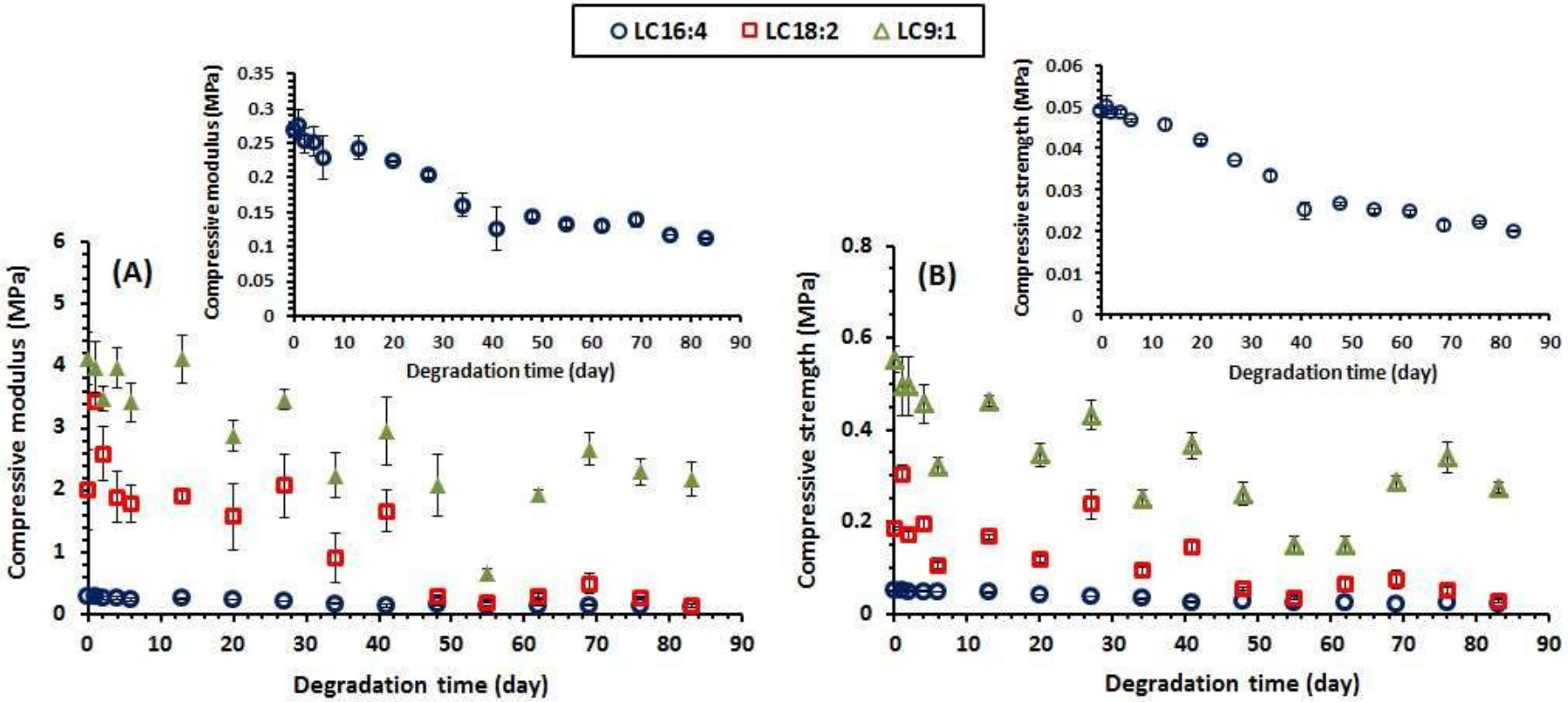

Figure 14: Retention of compressive modulus and strength for LC scaffolds versus degradation time. Compressive strength was determined as the maximum stress at strain of 20%. Compressive modulus and strength plots for LC16:4 scaffolds were magnified in the insert figures for ease of tracking as shown.

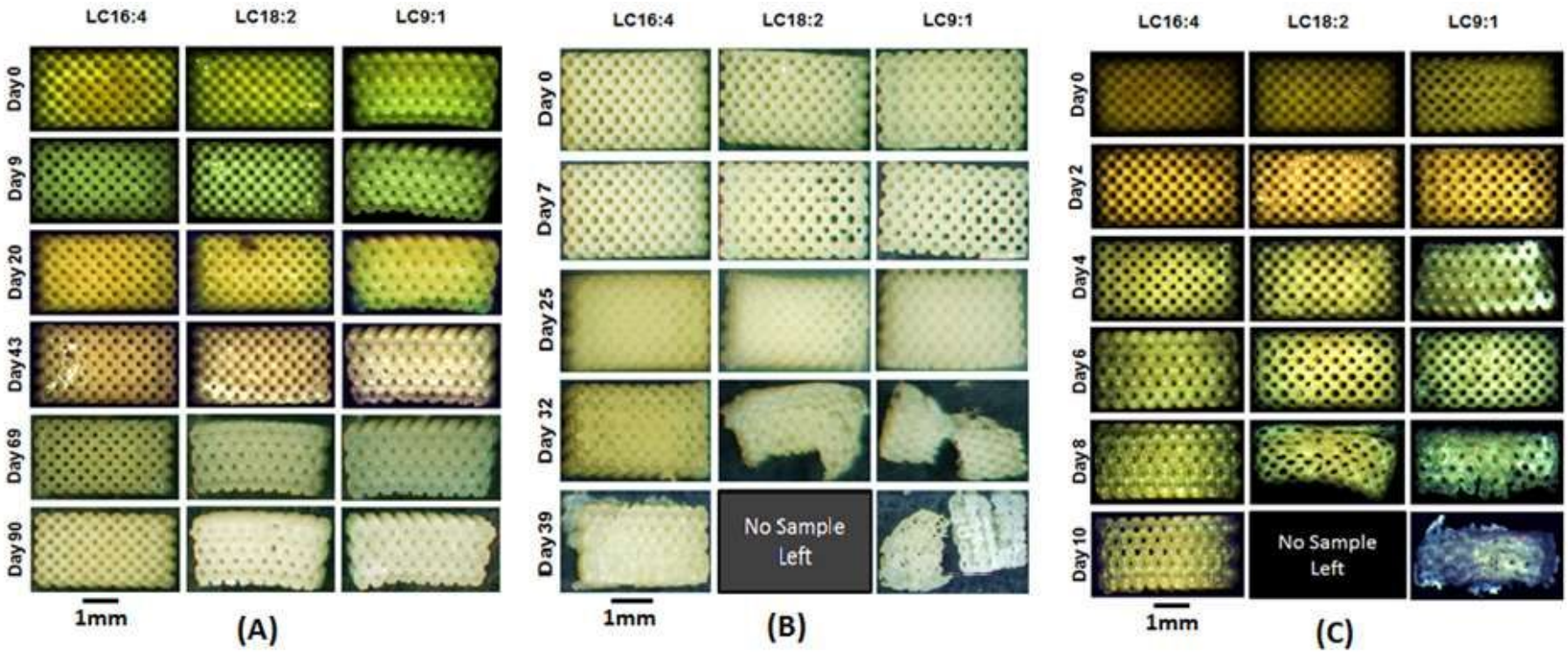

Figure 15: Optical images for LC scaffolds throughout in vitro degradation in PBS at different temperatures; (A) 37ºC, (B) 50ºC and (C) 65ºC. Scaffolds have a rectangular shape with dimensions of 2x4x2 mm^3. The change in the image colour was due to change of the microscope camera during the study.